Assimilation of surface velocities acquired between 1996 and 2010 to constrain the form of the basal friction law under Pine Island Glacier

F. Gillet-Chaulet, G. Durand, O. Gagliardini, C. Mosbeux, J. Mouginot, F. Rémy, C. Ritz

AGU PUBLICATIONS

Geophysical Research Letters

RESEARCH LETTER
10.1002/2016GL069937

Key Points:
- Assimilate Pine Island Glacier surface velocities to constrain basal friction changes
- Observed accelerations are consistent with a plastic deformation of subglacial sediments
- The response of ice streams to perturbations could be underestimated by most ice-sheet models

Supporting Information:
- Supporting Information S1

Correspondence to:
F. Gillet-Chaulet,
Fabien.Gillet-Chaulet@univ-grenoble-alpes.fr

Citation:
Gillet-Chaulet, F., G. Durand, O. Gagliardini, C. Mosbeux, J. Mouginot, F. Rémy, and C. Ritz (2016), Assimilation of surface velocities acquired between 1996 and 2010 to constrain the form of the basal friction law under Pine Island Glacier, *Geophys. Res. Lett.*, *43*, 10,311–10,321, doi:10.1002/2016GL069937.

Received 7 JUN 2016
Accepted 22 SEP 2016
Accepted article online 28 SEP 2016
Published online 13 OCT 2016

Assimilation of surface velocities acquired between 1996 and 2010 to constrain the form of the basal friction law under Pine Island Glacier

F. Gillet-Chaulet[1], G. Durand[1], O. Gagliardini[1], C. Mosbeux[1], J. Mouginot[2], F. Rémy[3], and C. Ritz[1]

[1]University of Grenoble Alpes, CNRS, IRD, IGE, Grenoble, France, [2]Department of Earth System Science, University of California, Irvine, California, USA, [3]Laboratoire d'Etudes en Géophysique et Océanographie Spatiale (CNRS-CNES-UPS-IRD), Toulouse, France

Abstract In ice-sheet models, slip conditions at the base between the ice and the bed are parameterized by a friction law. The most common relation has two poorly constrained parameters, C and m. The basal slipperiness coefficient, C, depends on local unobserved quantities and is routinely inferred using inverse methods. While model results have shown that transient responses to external forcing are highly sensitive to the stress exponent m, no consensus value has emerged, with values commonly used ranging from 1 to ∞ depending on the slip processes. By assimilation of Pine Island Glacier surface velocities from 1996 to 2010, we show that observed accelerations are best reproduced with $m \geq 5$. We conclude that basal motion, in much of the fast flowing region, is governed by plastic deformation of the underlying sediments. This implies that the glacier bed in this area cannot deliver resistive stresses higher than today, making the drainage basin potentially more sensitive to dynamical perturbations than predicted with models using standard values $m = 1$ or 3.

1. Introduction

Motion of fast-flowing ice streams found within polar ice sheets is largely determined by ice slipping over underlying bed materials. Constraining the conditions at the base remains a challenge for ice-flow models as they involve complex interactions between the ice, the bed which can be rigid or composed of soft sediments, and the basal hydrology [*Vaughan and Arthern*, 2007]. This wide range of interacting processes makes the basal conditions highly variable in space and time [*Clarke*, 2005].

Broadly, basal slip is usually divided into two large classes depending if the bed is hard or soft [*Cuffey and Paterson*, 2010]. Hard bed sliding is controlled by the ice deformation over the surface rugosity which itself can be effectively smoothed by cavity formation [e.g., *Schoof*, 2005], while soft bed sliding is controlled by the deformation of the underlying sediments which depends on the physical properties of the till (porosity, diffusivity, dilatancy, grain shape and size distributions, etc.) and the water pressure [*Tulaczyk et al.*, 2000a]. Progress with theoretical and numerical models has been made to physically include these processes [e.g., *Schoof*, 2005; *Gagliardini et al.*, 2007; *Damsgaard et al.*, 2015]. It remains challenging, however, to implement these processes in large-scale ice-sheet models both because of their numerical cost and because the introduction of additional poorly constrained parameters.

Basal slip in ice-flow models is represented by a friction law, i.e., a relationship between basal velocity $\boldsymbol{u}_b$ and basal shear stress $\boldsymbol{\tau}_b$. The most commonly used relation is the nonlinear Weertman law:

$$\boldsymbol{u}_b + C|\boldsymbol{\tau}_b|^{m-1}\boldsymbol{\tau}_b = 0 \quad (1)$$

where m is the stress exponent and the basal slipperiness coefficient, C, is a positive scalar representative of local properties of the bed (rugosity, water pressure, nature of the bed, etc.) assumed here independent of u_b and τ_b. Equation (1) was originally developed to represent the creep of ice over rough hard beds [*Weertman*, 1957]; the value of m is then equal to the creep exponent n entering the ice constitutive rheological relation and usually taken equal to 3. However, the same friction law can be used to represent different processes depending on the value of m; small values ($m \leq 3$) have been suggested to represent a viscous deformation

of the subglacial till [*Hindmarsh*, 1997], while equation (1) with $m \to \infty$ mimics plastic behavior, i.e., $\tau_b = C$ste and thus can represent plastic deformation of the till or ice flowing over a rigid bed with filled cavities [*Schoof*, 2005].

As direct observations of the conditions at the bed are very sparse, no consensus on the value of m has emerged and values ranging from 1 to ∞ are commonly used in flow models used to predict the future contribution of polar ice sheets to sea level rise (SLR). As shown recently, such projections are highly sensitive to m, with nonlinear relationships leading to higher contributions [*Ritz et al.*, 2015] as perturbations at the ice-sheet margins are transmitted farther and faster inland [*Price et al.*, 2008]. Reduction of uncertainties in SLR projections requires improved constraints on the friction law.

Formal inverse methods are routinely used to tune C, so that model surface velocities match the observations [e.g., *Joughin et al.*, 2009; *Morlighem et al.*, 2010; *Favier et al.*, 2014]. However, for a given unique set of observations, the inferred basal stress must satisfy the global stress balance, so the solution of the inverse problem leads to the same basal stress whatever the value of m [*Joughin et al.*, 2004]. Constraining m then requires observations at different times with significant differences in basal velocities and/or stresses. *Jay-Allemand et al.* [2011] use a 10 year data set to explore changes in basal conditions prior to and during the 1982–1983 surge of Variegated glacier (Alaska). They assume $m = 3$ and interpret changes in τ_b in terms of changes in C associated with changes of the basal water pressure. *Habermann et al.* [2013] show that changes in basal stresses in Jakobshavn Isbrae (Greenland) between 1985 and 2008 are correlated with changes in height above flotation and thus consistent with a plastic Mohr-Coulomb parameterization of τ_b. *Minchew et al.* [2016] show that seasonal flow variations of Hofsjökull Ice Cap (Iceland) can be explained by a bed deforming plastically and weakening with increased meltwater supply in summer. All these studies are in areas where we can expect changes in water conditions at the bed either because of the proximity to the ocean or because of variability in surface meltwater supply and routing, so that changes due to the nonlinearity of the friction law cannot be unambiguously separated from changes in water conditions.

For constant basal properties, variations of the stress regime sufficient to significantly affect flow velocities can then only be obtained in response to tidal forcing or to changes in longitudinal and gravitational stresses induced by the transmission of dynamical perturbations, e.g., ungrounding or ice shelf thinning. Using a viscoelastic model of coupled ice shelves/ice streams, *Gudmundsson* [2007, 2011] and *Rosier et al.* [2014, 2015] show that ice flow modulations in response to tidal forcing in Rutford Ice Stream (Antarctica) can only be reproduced with nonlinear friction laws ($m > 1$) and found a best match for $m \approx 3$. A nearly twofold speedup has been observed in Pine Island Glacier (PIG) between 1974 and 2010, making it the largest contributor to SLR in Antarctica [*Mouginot et al.*, 2014]. Speedup has propagated to most of the drainage basin and has also induced important changes in surface elevation and slope [*Scott et al.*, 2009; *Wingham et al.*, 2009; *Flament and Rémy*, 2012]. *Joughin et al.* [2010] found that the observed dynamic thinning in PIG in response to the observed grounding line retreat is better reproduced with a model where hard beds follow equation (1) with $m = 3$ and where soft beds deform plastically.

Here we formulate an inverse problem to constrain m from the observations of surface velocities and elevation in PIG between 1996 and 2010. By definition, the basal friction becomes null where the ice detaches from the bed and goes afloat, i.e., at the grounding line. As the results could be perturbed by errors in the grounding line position, we restrict our study to the upper part of the drainage basin, some 30 km upstream from the grounding line (Figure 1a). While indirect observations of subglacial lake drainages are evidences for a dynamic subglacial water system even in areas not affected by surface melt [*Fricker et al.*, 2007; *Flament et al.*, 2014], on this time scale, we neglect changes in subglacial hydrology and lithology. In other words, we assume in the model that the material properties that can affect basal slip, represented by the basal slipperiness coefficient, C, in equation (1), are function of space only, so that changes in the basal stress, τ_b, can only be induced by changes in basal velocity, u_b. Under these assumptions, we test the ability of the flow model to reproduce observed velocity changes with a Weertman friction law (1) and a uniform value of m.

2. Methodology

We use the finite element ice flow model Elmer/Ice [*Gagliardini et al.*, 2013] to infer the basal friction relation under PIG. Data sets used in this study and the main model assumptions are summarized below.

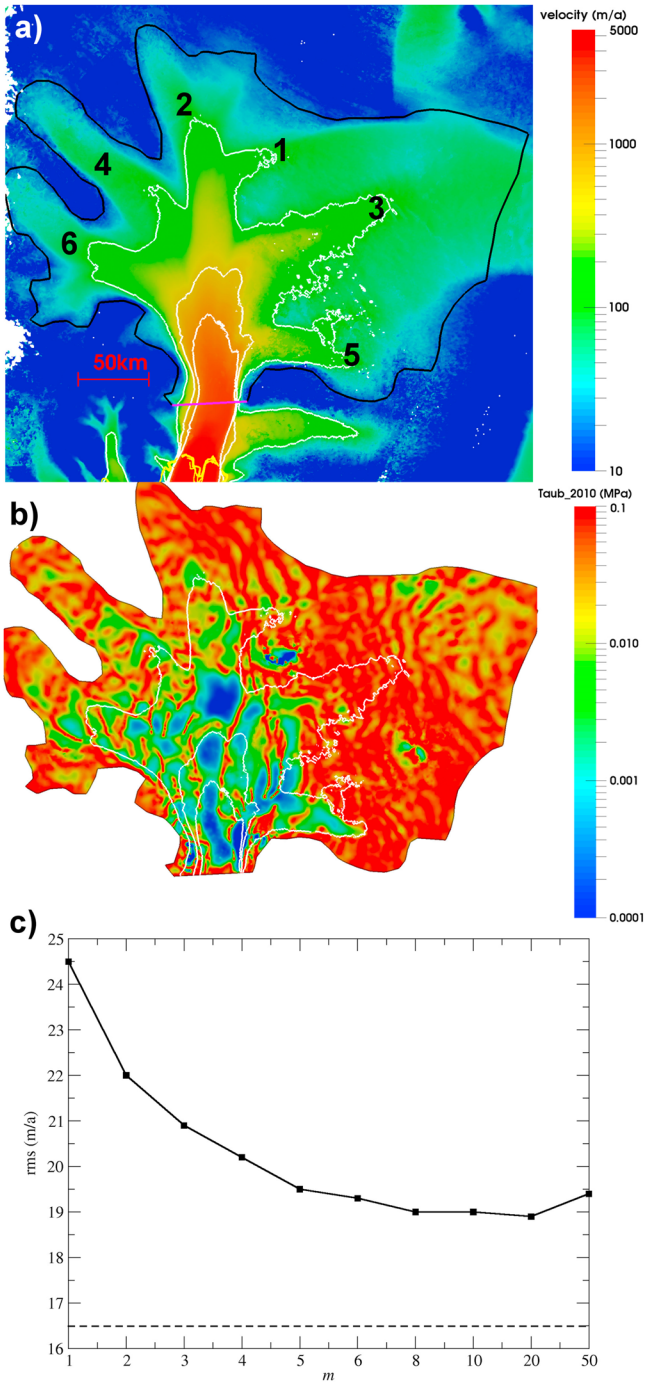

Figure 1. (a) Observed surface velocity [*Rignot et al.*, 2011a]. The white lines are the 100, 500, and 1000 m/a contours. The model domain is delimited by the black and magenta lines which denote two different boundary conditions (see text). Measured grounding lines (1992 to 2009) are in yellow [*Rignot et al.*, 2011b]. Numbers 1–6 denote the tributaries discussed in the main text and follow *Rippin et al.* [2011]. (b) Basal stress τ_b inferred for 2010 with $m = 20$. (c) RMSE as a function of m. The dashed line shows the RMSE (independent of m) obtained when inverting each year individually. Values are given in Table S1.

2.1. Data Sets
2.1.1. Velocities

Interferometric synthetic aperture radar data acquired during the 2007–2009 International Polar Year have allowed for a nearly complete high resolution digital mosaic of surface velocity for all Antarctica [*Rignot et al.*, 2011a; *Mouginot et al.*, 2012]. Reported errors range from 1 m/a to 17 m/a in coastal areas. Individual mean

annual velocity maps are often incomplete and, for our study, we have selected five data sets (1996 and from 2007 to 2010) with good spatial coverage in PIG drainage basin. For 1996, velocity has been measured from ascending/descending interferometric phases acquired by ERS/ESA, while for 2007 to 2010 it has been measured from speckle tracking using ALOS-PALSAR/JAXA. The velocity from the mosaic map is shown in Figure 1a, while velocity changes between 1996 and 2010 are shown in Figure 2a.

2.1.2. Topography

Changes in ice surface elevation can be accurately measured by satellite radar altimeters. Precise along-track processing of the Envisat data set from 2002 to 2010 has confirmed that dynamic thinning in PIG is accelerating and propagating upstream [*Flament and Rémy*, 2012]. For each year, we compute the annual mean surface elevation using ERS1 for 1996 and Envisat for 2002 to 2010. Elevation differences are then interpolated at the model grid nodes to correct the surface elevation given by the reference Antarctic topography data set Bedmap2 [*Fretwell et al.*, 2013]. While it uses data from different dates, the Bedmap2 surface elevation is tagged for 2004. Interpolating surface elevation differences rather than annual elevations gives smoother surface elevations and leads to smaller root-mean-square errors (RMSE) between observed and model velocities but does not affect the interpretation of the results. Along-track surface elevation differences, together with velocity differences, between 2010, 2008, 2007, and 1996, are shown in Figure S1 in the supporting information. The bedrock elevation is given by Bedmap2 [*Fretwell et al.*, 2013].

2.2. Model Description

As solving the full set of mechanical equations (3-D Stokes equations) remains computationally expensive, all results presented here have been computed using the depth-averaged shallow-stream approximation equations [e.g., *MacAyeal*, 1989]. However, the robustness of our conclusions has been validated by running few experiments with the 3-D Stokes model. More details on the model used here can be found in *Fürst et al.* [2015].

2.2.1. Constitutive Relations

The constitutive relation for ice rheology is given by the standard isotropic, nonlinear Glen's flow law with a stress exponent $n = 3$. The ice viscosity parameter depends on the temperature following an Arrhenius relation [*Cuffey and Paterson*, 2010]. The englacial temperature field is assumed to be constant over the short period studied here and is given by a temperature reconstruction [*Van Liefferinge and Pattyn*, 2013]. The basal friction law is given by equation (1).

2.2.2. Model Domain and Boundary Conditions

The model domain, shown in Figure 1a, is restricted to the fast-flowing area. The sides (black line) correspond approximately to the 25 m/a velocity contour, and the downstream boundary in the main trunk (magenta line) is upstream of a tributary and ~ 30 km from the grounding line. Dirichlet conditions for the ice velocity are applied on all boundaries. They are given by annual velocity maps in the main trunk (downstream boundary) and by the velocity mosaic at the sides as, here, the coverage of the annual maps is not always complete and, where available, velocity differences between 1996 and 2010 are within the uncertainty (see Figure S1). The domain is meshed using anisotropic triangular elements ranging from ~500 m in the fastest-flowing regions to ~1500 m in the most upstream part. This results in a total of ~61,000 mesh nodes.

2.2.3. Inverse Method

A control inverse method is used to constrain the basal slipperiness coefficient C in equation (1) so that the misfit between model and observed velocities is minimized. For each year Y = (1996, 2007, 2008, 2009,and 2010), a cost function is defined as follows:

$$J_Y(C(Y,x,y)) = \sum_{i=1}^{N_Y^{\mathrm{obs}}} 0.5 \|\boldsymbol{u}_i^{\mathrm{model}} - \boldsymbol{u}_i^{\mathrm{obs}}\|^2 \tag{2}$$

where N_Y^{obs} is the number of observation points for year Y, $\boldsymbol{u}_i^{\mathrm{obs}}$ and $\boldsymbol{u}_i^{\mathrm{model}}$ are the observed and model horizontal surface velocities at observation point i. The RMSE between the model and the observations is then simply given as $\mathrm{RMSE}_Y = \sqrt{2J_Y/N_Y^{\mathrm{obs}}}$.

As mentioned previously, when several data sets are available, it is common to invert the basal stress field for each data set and interpret local changes in τ_b [*Jay-Allemand et al.*, 2011; *Habermann et al.*, 2013; *Minchew et al.*, 2016]. Solved independently, the five inverse problems (2) are independent of m as the inverse method should lead to the same effective basal slipperiness $C_{\mathrm{eff}}(Y,x,y) = C[\tau_b(Y,x,y)]^{m-1}\ \forall m$. However, this relation

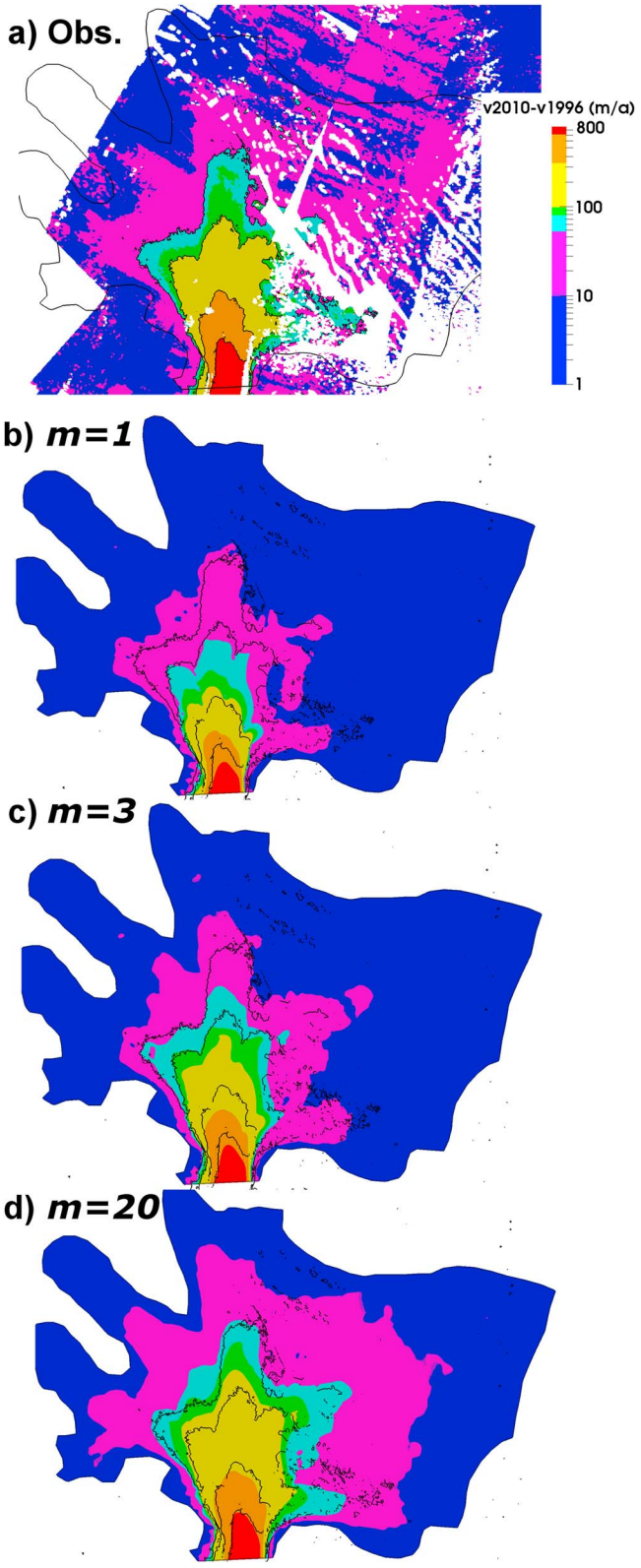

Figure 2. Velocity differences between 2010 and 1996 (a) observed and as given by the model for (b) $m=1$, (c) $m=3$, and (d) $m=20$. Isolines of observed 50, 100, 300, and 600 m/a differences are reported in each subfigure. Complementary results for m = 5, 10, and 50 are shown in Figure S3.

could be used to infer mean (time independent) values of $C(x, y)$ and $m(x, y)$ at every mesh node from the five solutions $[C_{\text{eff}}(Y, x, y), \tau_b(Y, x, y)]$. As common, the solution of the inverse problem is not unique, and values of τ_b can vary by orders of magnitude with little effect on surface velocities and on the value of the cost function [*Jay-Allemand et al.*, 2011]. This is particularly true in areas of weak bed where only a small fraction of the driving stress is supported. It would then be difficult to estimate the uncertainties attached to the values of C and m inferred with this method.

To overcome this difficulty, we further decrease the number of degrees of freedom and assume that m is uniform in our model domain, as common in most ice-sheet models. For a given m, the mean basal slipperiness coefficient $C_m(x, y)$ that best matches the observations can then be estimated from a new inverse problem where the cost function is given by

$$J_T(C_m(x, y)) = J_{1996} + J_{2007} + J_{2008} + J_{2009} + J_{2010}. \quad (3)$$

We test different values of m. Solutions matching the observations within observational errors will allow to validate our assumptions (the basal material properties have not changed and m is uniform) and estimate best values for m. For a given m, the minimum of J_T that can be achieved by the inverse model is usually obtained when no a priori assumption on the spatial variations of C is made, i.e., when no regularization is added to the cost function. However, for high values of m the nonlinearity of the problem increases and the computation of the gradient becomes less accurate, which can affect the efficiency of the minimization algorithm. In what follows we always report the minimum of J_T and, for $m \geq 8$, this minimum was found with a small regularization term penalizing the first spatial derivative of $\log_{10}(C)$.

3. Results

There is no accurate estimate of the observational errors. However, using a twin experiment with random errors, *Arthern and Gudmundsson* [2010] have shown that the RMSE slightly overfit the noise level. Here the RMSE obtained by solving the five inverse problems (equation (2)) independently corresponds to the minimum that can be achieved with the same model configuration and should give a lower bound for the observational error. For the 5 years together it is 16.5 m/a. While it is slightly higher than the data uncertainty reported in the area [*Mouginot et al.*, 2012], it is similar to RMSE reported by other studies [*Morlighem et al.*, 2010; *Fürst et al.*, 2015].

The minimum of J_T (equation (3)) as a function of m is shown in Figure 1c. Values for individual years are given in supporting information Table S1. The RMSE decreases substantially from 24.5 m/a with $m = 1$ to 19.5 m/a for $m = 5$ then decreases less rapidly for larger values of m. A minimum of 18.9 m/a is obtained for $m = 20$. It increases again to 19.4 m/a for $m = 50$. The solution is mainly driven by observations from 2007 to 2010 as they show velocities significantly higher than in 1996. As a consequence, the decrease is more pronounced for J_{1996}, from 34.3 m/a for $m = 1$ to 17.5 m/a for $m = 20$. For years 2007 to 2010, the RMSE is fairly independent of m within ± 0.5 m/a for $m > 4$.

The 2010 basal stress obtained with $m = 20$ is shown in Figure 1b and agrees with previous studies [*Vieli and Payne*, 2003; *Joughin et al.*, 2009; *Morlighem et al.*, 2010]. Fastest flow velocities under the main trunk correspond to very low basal stresses (<1 kPa), and in general, velocities faster than 100 m/a are well correlated with a basal stress lower than 10 kPa, with a notable exception for the tributary 3. Sticky spots with higher basal stress forming bands similar to those observed by *Sergienko et al.* [2014] are also present within the areas of low basal stress. Lower velocities correspond to basal stresses of the order of 100 kPa or more.

Maps of observed and model velocity changes between 1996 and 2010 for $m = 1, 3, 20$ are shown in Figure 2, while the mean flow accelerations for all the points within the model domain are shown in Figure 3. The same two figures for $m = 5, 10, 50$ are given in Figures S3 and S4. The flow accelerations have often been illustrated along the central flow line only [e.g., *Joughin et al.*, 2010; *Mouginot et al.*, 2014]; here we show that over the 1996–2010 period, the mean flow acceleration is surprisingly proportional to the 2010 velocities over the whole model domain, with an average rate of 2.4% a^{-1}. It is slightly higher at 3% a^{-1} for the period 2007–2010. These values are in agreement with values published elsewhere [*Joughin et al.*, 2003; *Scott et al.*, 2009; *Joughin et al.*, 2010; *Mouginot et al.*, 2014] and the mean increase in surface slope of 1% per year in most of the drainage basin reported for the period 2002–2010 [*Flament and Rémy*, 2012]. Over the shortest time periods (2008–2010 and 2009–2010) the rate is smaller especially for the fastest (and thus most downstream)

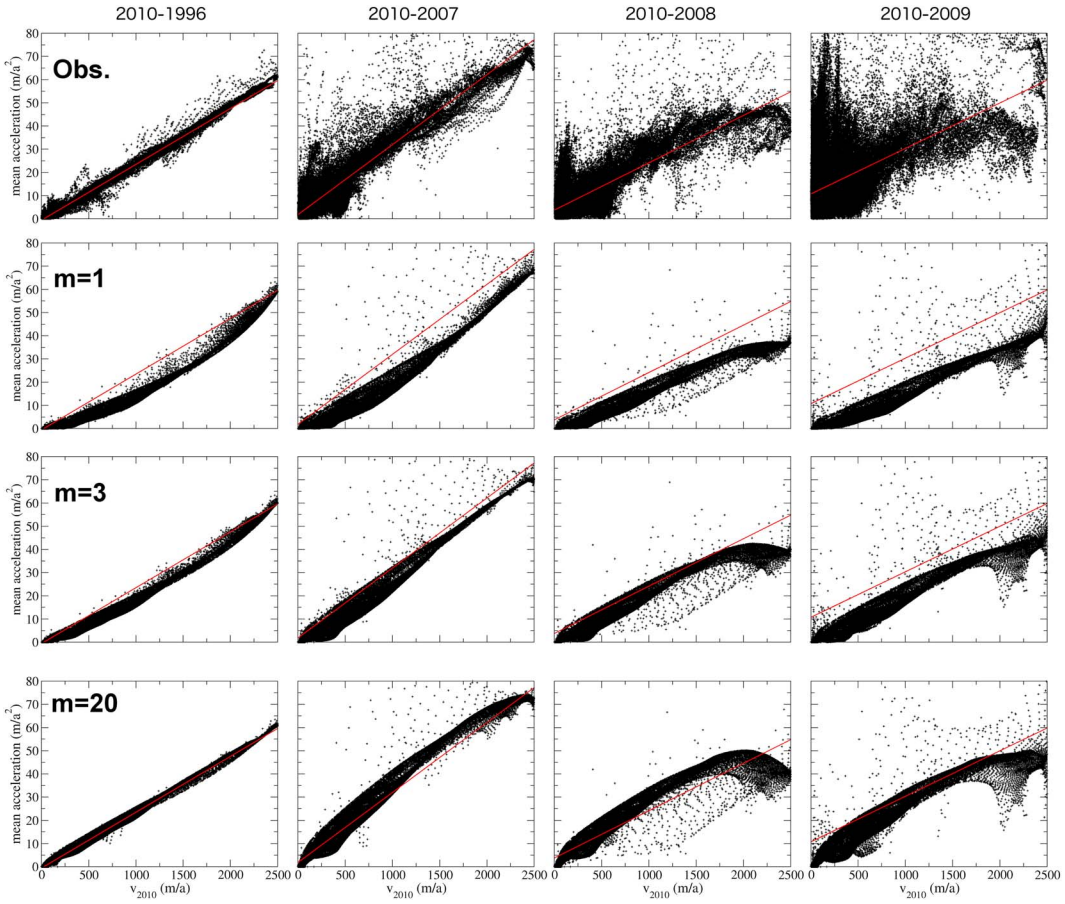

Figure 3. Mean acceleration, $\Delta u/\Delta t$, between 2010 and the four other years (1996, 2007, 2008, and 2009) as a function of the 2010 velocity for each observation within the model domain and for the model at each mesh node with $m=1$, $m=3$, and $m=20$. Red lines are linear regressions of the observations. Complementary results for m = 5, 10, and 50 are shown in Figure S4.

velocities in agreement with a stabilization of the ice discharge in 2010 [*Mouginot et al.*, 2014]. The pattern and the magnitude of the velocity changes are well reproduced with $m=20$, while acceleration rates are underestimated over the whole domain and for all time periods with $m \leq 3$. Differences between the results are less important for $m \geq 5$; however, larger values produce larger and more upstream accelerations. This is particularly visible over the shortest time periods, but the accuracy of the data compared to observed changes is not sufficient to discriminate the results for $m \geq 5$. The most notable difference in the velocity change pattern as m is increased is the higher changes in the south (right-hand side of Figure 2), especially in tributaries 3 and 5, and in areas of higher basal stress. This speedup is not clear in the velocity observations because of missing data; however, it is supported by the important thinning that is also propagating to this area (Figure S1).

4. Discussion

With the inverse problem formulated here, the uncertainty associated with our assumptions on C and m has been directly quantified in terms of error on the variable that is effectively observed, i.e., surface velocity. The RMSE increases from 16.5 m/a with no assumption to a minimum of 18.9 with a uniform value $m=20$ and $C(Y,x,y)=C(x,y)\ \forall Y$. Because velocity differences are close to the observational noise in a large part of the model domain, the RMSE does not allow to discriminate between the results for $m \geq 5$, however, in general, the speedup given by the model increases with m. A more accurate determination of m would require longer time series.

Using equation (1), it can be shown that a twofold speedup induces only a 3.5% increase in basal stress with $m=20$ (respectively, 7.2% and 14.9% with $m=10$ and $m=5$). The mean difference over all the mesh nodes between τ_b^{1996} and τ_b^{2010} is only 3.5 kPa with $m=20$ (see Figure S2). We conclude that velocity observations

in PIG drainage basin in 1996 and from 2007 to 2010 are better reproduced if basal shear stresses are quasi-independent of basal velocities, implying a quasi-plastic behavior. The robustness of this result has been evaluated by running experiments with uniform enhancement factors to the ice fluidity equals respectively to 0.5 and 2.5. The same dependency of J_T to m has been observed. Solving the full set of mechanical equations (Stokes equations without approximation), but on a mesh of lower resolution, also shows a decrease of J_T from 23.9 m/a for $m=1$ to 21.1 m/a for $m=5$ (for a minimum of 18.2 m/a when solving the five inverse problems (2) independently). The need of quasi-constant basal stresses also emerges when comparing values inverted for years 1996 and 2010 individually as they broadly follow the line $\tau_b^{2010}=\tau_b^{1996}$ (see Figure S2). However, the spread is very large and locally inverted values can change by orders of magnitude, showing the difficulty in interpreting local changes in basal stresses solutions of the inverse problem. The high nonlinearity of the friction law (1) makes the drainage basin particularly sensitive to dynamical perturbations, as additional stresses have to be either compensated by increased basal stresses implying a large increase in basal sliding, or transmitted inland to the upstream boundaries.

In the same section of PIG, *Joughin et al.* [2003] and *Scott et al.* [2009] found that the acceleration along the central flow line can be explained by the increase in driving stress produced by the steepening of the surface, without local sustained reduction in basal stresses or increase in longitudinal stresses. To evaluate the contribution to the observed acceleration of (i) increased driving stresses and (ii) increased longitudinal stresses transmitted from the downstream boundary, we have run two additional experiments with $m=20$: in the first, the boundary condition in the main trunk (magenta line in Figure 1a) is kept the same and given by the velocity mosaic, while in the second the surface elevation is the same for all years and given by Bedmap2. Model velocity changes between 1996 and 2010 are given in Figure S5. It shows that changes in most of the basin (up to ~100 m/a) are explained by changes in surface elevation only and thus the progressive upstream diffusion of increased driving stresses. However, the loss of buttressing at the downstream boundary, represented by the increased velocities at the boundary, is directly transmitted inland by increased longitudinal stress gradients and explain a large part of the velocity changes up to ~100 km upstream. This is in agreement with the synchronous short-term accelerations recorded by *Scott et al.* [2009] on two GPS in the central flow line, located 55 km and 111 km upstream of the grounding line.

Seismic and airborne potential field data close to the junction of tributaries 2, 3, and 4 have shown that the majority of the bed is made of soft, water-saturated deforming sediments with patches of nondeforming sediments and maybe water [*Smith et al.*, 2013]. *Rippin et al.* [2011] used airborne radio echo sounding to map the basal roughness under PIG. They found a large zone of low basal roughness under the main trunk interpreted as indicative of significant marine sediments deposited following the disappearance of the West Antarctic Ice Sheet 200 ka before present. They found that the majority of the tributaries are rougher but with a relatively high variability. Basal roughness is well correlated with basal drag inferred from previous inversions studies [*Vieli and Payne*, 2003; *Joughin et al.*, 2009; *Morlighem et al.*, 2010], with high roughness corresponding to high basal stress and inversely. *Wilkens et al.* [2015] study two different parameterizations of the basal slipperiness from the basal roughness. They show that this allows to reproduce the most important features of the flow but not all the details. Here we found also that, in general, small basal stresses correspond to small basal roughness. However, the spread remains too large to propose a parameterization of the basal stress as a function of the basal roughness only. Following these previous studies, as most of the changes have happened in the main trunk where we found high velocities and low basal stress, we interpret our results as mostly representative of the deformation of soft sediments beneath the main trunk.

Numerous laboratory studies on till samples and in situ measurements have shown that at large strain the till rheology is plastic with a critical strength $\tau*$ well described by a Mohr-Coulomb criterion (see, e.g., reviews from *Murray* [1997], *Clarke* [2005], *Iverson* [2010], and *Cuffey and Paterson* [2010]):

$$\tau* = c + N\tan\phi \tag{4}$$

with c the cohesion, ϕ the friction angle and $N = p_i - p_w$ the effective pressure where p_i and p_w are the ice overburden pressure and the water pressure, respectively. However, it has been suggested that at large spatial and temporal scale the resulting apparent behavior could appear as viscous [*Hindmarsh*, 1997; *Fowler*, 2003], which has motivated the use of small values of m in large-scale flow models even to represent basal slip over soft beds. However, *Tulaczyk* [2006] has shown that GPS measurements of stick-slip events in Whillans Ice Stream where consistent with the plastic rheology inferred from laboratory measurements. The friction law (1) mimics the Coulomb rheology (equation (4)) for $m \to \infty$ and $C^{-1/m}=\tau*$. The good agreement between

the model and the observations, obtained only for $m \geq 5$, then supports a quasi-plastic behavior described by equation (4). The effective pressure can then be estimated form equation (4), if we take $\tau_b = \tau *$ and assume negligible cohesion and tan $\phi = 0.4$ as in *Minchew et al.* [2016]. We found that in most of the model domain, N is only a small fraction of the ice overburden pressure $p_i \approx \rho_i g h$, with ρ_i the ice density and h the ice thickness. It involves that the effective pressure could be substantially affected by small changes in p_i and/or p_w. Changes in ice thickness between 1996 and 2010 have not exceeded 2%. The hydrological conditions at the base of the ice sheet are mostly unknown, so that the basal water pressure p_w cannot be estimated independently; however, our results indicate that most of the observations can be explained with quasi-constant basal stresses, implying quasi-constant effective pressures. It is expected that the basal water pressure could change in response to changes in hydraulic potential induced by changes in driving stresses or changes in basal melt rates induced by changes in frictional heating, creating potentially important feedbacks [e.g., *Tulaczyk et al.*, 2000b]. However, constraining such feedbacks will certainly require longer time series and additional geophysical investigations through borehole instrumentation, for example.

Joughin et al. [2010] compared the response of PIG drainage basin to observed retreat of the grounding line using three sliding parameterizations: linear viscous ($m = 1$), plastic ($m = \infty$) and mixed (plastic for soft bed ($\tau_b < 40$ kPa), $m = 3$ elsewhere). They found that the linear viscous model underpredicts inland thinning as observed from surface altimetry. This is in line with our results showing that the speedup cannot be reproduced with low values of m. On the contrary, their purely plastic model does not reproduce the near grounding line thinning and seems to overpredict inland thinning, while their mixed model is in good agreement with the observations along the central trunk. While we cannot impose variable values of m in our model, the fact that velocity changes are underestimated with $m = 3$ also in areas of high basal stress (see particularly tributary 3) seems not consistent with a transition at 40 kPa. However, very large values of m seem to overpredict the inland acceleration (see results for $m = 50$ in Figures S3 and S4), supporting a not fully plastic behavior at large basal stresses. The applicability of a simple friction law (1) with a uniform value of m at high basal stresses may be more uncertain as a variety of processes may lead to high friction. *Smith et al.* [2013] identify a geological boundary bellow the main trunk of PIG where contrasting basal stresses and velocity patterns correlate with changes in subglacial geology deeper than the ice-bed interface. The acoustic properties of the interface do not change across the boundary; however, the sediment layer gets thinner (<10 m), leading to higher basal roughness, higher basal stress, and lower ice velocity. In addition, *Stokes et al.* [2007] review different types of sticky spots that have been identified in both contemporary and paleo–ice streams (bedrock bumps, till-free areas, drained strong till, and freeze-on of subglacial water). We may anticipate that these different beds could respond differently to external changes. Efforts to constrain m in areas of high basal stresses will require longer time series to get velocity changes significantly higher that the measurement uncertainties; however, they could be compromised by poorly constrained thermomechanical feedbacks between the ice and the bed.

5. Conclusion

With the assumption that the basal slipperiness coefficient, C, has been constant in time between 1996 and 2010, we have been able to reproduce most of the observed velocity changes in PIG with the basal friction law that is commonly used in ice-sheet models. The best match is obtained for a constant value of the stress exponent $m = 20$ with a RMSE of 18.9 m/a, while with a value of C that can vary with time (i.e., unique spatial fields for each velocity data set) the minimum improves only slightly to 16.5 m/a. Differences in RMSE are very low for $m \geq 5$; however, there is still differences in the pattern and magnitude of the speedup, larger values leading to larger and more upstream speedup. The linear viscous ($m = 1$) or slightly nonlinear ($m = 3$) laws, which are the most commonly used relations in flow models, provide a poorer fit to the observations.

These results are mostly representative of the behavior of the sediments that have been observed below PIG, and their wide applicability will have to be tested in other areas and against longer time series. However, ice streams with weak beds are common in Antarctica and also maybe more than previously thought in Greenland [*Shapero et al.*, 2016].

This results is important for large-scale flow models predicting the dynamic contribution of polar ice sheets to SLR as nonlinear relations favor inland propagation of dynamical perturbations at the margins [*Price et al.*, 2008], influence marine ice-sheet profiles and stability [*Tsai et al.*, 2015; *Robel et al.*, 2016] and lead to higher SLR contributions [*Ritz et al.*, 2015].

Acknowledgments
This work was supported by French National Research Agency (ANR) under the SUMER (Blanc SIMI 6) 2012 projectANR-12-BS06-0018. LGGE is part of Labex OSUG@2020 (ANR10 LABX56). Most of the computations presented in this paper were performed using the Froggy platform of the CIMENT infrastructure (https://ciment.ujf-grenoble.fr), which is supported by the Rhône-Alpes region (GRANT CPER07-13 CIRA), the OSUG@2020 labex (reference ANR10 LABX56), and the Equip@Meso project (reference ANR-10-EQPX-29-01) of the programme Investissements d'Avenir supervised by the Agence Nationale pour la Recherche. The data used are listed in the references. The authors thank the three anonymous reviewers for their constructive comments.

References

Arthern, R. J., and G. H. Gudmundsson (2010), Initialization of ice-sheet forecasts viewed as an inverse Robin problem, *J. Glaciol.*, *56*(197), 527–533.
Clarke, G. K. (2005), Subglacial processes, *Annu. Rev. Earth Planet. Sci.*, *33*(1), 247–276, doi:10.1146/annurev.earth.33.092203.122621.
Cuffey, K. M., and W. S. B. Paterson (2010), *The Physics of Glaciers*, Academic Press, New York.
Damsgaard, A., D. L. Egholm, J. A. Piotrowski, S. Tulaczyk, N. K. Larsen, and C. F. Brædstrup (2015), A new methodology to simulate subglacial deformation of water-saturated granular material, *Cryosphere*, *9*(6), 2183–2200, doi:10.5194/tc-9-2183-2015.
Favier, L., G. Durand, S. L. Cornford, G. H. Gudmundsson, O. Gagliardini, F. Gillet-Chaulet, T. Zwinger, A. J. Payne, and A. M. Le Brocq (2014), Retreat of Pine Island Glacier controlled by marine ice-sheet instability, *Nat. Clim. Change*, *4*(2), 117–121, doi:10.1038/nclimate2094.
Flament, T., and F. Rémy (2012), Dynamic thinning of Antarctic glaciers from along-track repeat radar altimetry, *J. Glaciol.*, *58*(211), 830–840.
Flament, T., E. Berthier, and F. Rémy (2014), Cascading water underneath Wilkes Land, East Antarctic ice sheet, observed using altimetry and digital elevation models, *Cryosphere*, *8*(2), 673–687.
Fowler, A. C. (2003), On the rheology of till, *Ann. Glaciol.*, *37*(1), 55–59, doi:10.3189/172756403781815951.
Fretwell, P., et al. (2013), Bedmap2: Improved ice bed, surface and thickness datasets for Antarctica, *Cryosphere*, *7*(1), 375–393, doi:10.5194/tc-7-375-2013.
Fricker, H. A., T. Scambos, R. Bindschadler, and L. Padman (2007), An active subglacial water system in West Antarctica mapped from space, *Science*, *315*(5818), 1544–1548.
Fürst, J. J., G. Durand, F. Gillet-Chaulet, N. Merino, L. Tavard, J. Mouginot, N. Gourmelen, and O. Gagliardini (2015), Assimilation of Antarctic velocity observations provides evidence for uncharted pinning points, *Cryosphere*, *9*(4), 1427–1443, doi:10.5194/tc-9-1427-2015.
Gagliardini, O., D. Cohen, P. Råback, and T. Zwinger (2007), Finite-element modeling of subglacial cavities and related friction law, *J. Geophys. Res.*, *112*, F02027, doi:10.1029/2006JF000576.
Gagliardini, O., et al. (2013), Capabilities and performance of Elmer/Ice, a new-generation ice sheet model, *Geosci. Model Dev.*, *6*(4), 1299–1318, doi:10.5194/gmd-6-1299-2013.
Gudmundsson, G. H. (2007), Tides and the flow of Rutford Ice Stream, West Antarctica, *J. Geophys. Res.*, *112*, F04007, doi:10.1029/2006JF000731.
Gudmundsson, G. H. (2011), Ice-stream response to ocean tides and the form of the basal sliding law, *Cryosphere*, *5*(1), 259–270, doi:10.5194/tc-5-259-2011.
Habermann, M., M. Truffer, and D. Maxwell (2013), Changing basal conditions during the speed-up of Jakobshavn Isbræ, Greenland, *Cryosphere*, *7*(6), 1679–1692, doi:10.5194/tc-7-1679-2013.
Hindmarsh, R. C. A. (1997), Deforming beds: Viscous and plastic scales of deformation, *Quat. Sci. Rev.*, *16*, 1039–1056.
Iverson, N. R. (2010), Shear resistance and continuity of subglacial till: Hydrology rules, *J. Glaciol.*, *56*(200), 1104–1114.
Jay-Allemand, M., F. Gillet-Chaulet, O. Gagliardini, and M. Nodet (2011), Investigating changes in basal conditions of Variegated Glacier prior to and during its 1982–1983 surge, *Cryosphere*, *5*(3), 659–672, doi:10.5194/tc-5-659-2011.
Joughin, I., E. Rignot, C. E. Rosanova, B. K. Lucchitta, and J. Bohlander (2003), Timing of recent accelerations of pine Island Glacier, Antarctica, *Geophys. Res. Lett.*, *30*(13), 1706, doi:10.1029/2003GL017609.
Joughin, I., D. R. MacAyeal, and S. Tulaczyk (2004), Basal shear stress of the Ross ice streams from control method inversions, *J. Geophys. Res.*, *109*, B09405, doi:10.1029/2003JB002960.
Joughin, I., S. Tulaczyk, J. L. Bamber, D. Blankenship, J. W. Holt, T. Scambos, and D. G. Vaughan (2009), Basal conditions for Pine Island and Thwaites Glaciers, West Antarctica, determined using satellite and airborne data, *J. Glaciol.*, *55*(190), 245–257.
Joughin, I., B. E. Smith, and D. M. Holland (2010), Sensitivity of 21st century sea level to ocean-induced thinning of Pine Island Glacier, Antarctica, *Geophys. Res. Lett.*, *37*, L20502, doi:10.1029/2010GL044819.
MacAyeal, D. R. (1989), Large-scale ice flow over a viscous basal sediment: Theory and application to ice stream B, Antarctica, *J. Geophys. Res.*, *94*(B4), 4071–4087, doi:10.1029/JB094iB04p04071.
Minchew, B., M. Simons, H. Björnsson, F. Palsson, M. Morlighem, H. Seroussi, E. Larour, and S. Hensley (2016), Plastic bed beneath Hofsjökull Ice Cap, central Iceland, and the sensitivity of ice flow to surface meltwater flux, *J. Glaciol.*, *62*(231), 147–158, doi:10.1017/jog.2016.26.
Morlighem, M., E. Rignot, H. Seroussi, E. Larour, H. B. Dhia, and D. Aubry (2010), Spatial patterns of basal drag inferred using control methods from a full-Stokes and simpler models for Pine Island Glacier, West Antarctica, *Geophys. Res. Lett.*, *37*, L14502, doi:10.1029/2010GL043853.
Mouginot, J., B. Scheuchl, and E. Rignot (2012), Mapping of ice motion in Antarctica using synthetic-aperture radar data, *Remote Sens.*, *4*(9), 2753–2767, doi:10.3390/rs4092753.
Mouginot, J., E. Rignot, and B. Scheuchl (2014), Sustained increase in ice discharge from the Amundsen Sea Embayment, West Antarctica, from 1973 to 2013, *Geophys. Res. Lett.*, *41*, 1576–1584, doi:10.1002/2013GL059069.
Murray, T. (1997), Assessing the paradigm shift: Deformable glacier beds, *Quat. Sci. Rev.*, *16*, 996–1016.
Price, S. F., H. Conway, E. D. Waddington, and R. A. Bindschadler (2008), Model investigations of inland migration of fast-flowing outlet glaciers and ice streams, *J. Glaciol.*, *54*(184), 49–60.
Rignot, E., J. Mouginot, and B. Scheuchl (2011a), Ice flow of the Antarctic ice sheet, *Science*, *333*(6048), 1427–1430, doi:10.1126/science.1208336.
Rignot, E., J. Mouginot, and B. Scheuchl (2011b), Antarctic grounding line mapping from differential satellite radar interferometry, *Geophys. Res. Lett.*, *38*, L10504, doi:10.1029/2011GL047109.
Rippin, D. M., D. G. Vaughan, and H. F. J. Corr (2011), The basal roughness of Pine Island Glacier, West Antarctica, *J. Glaciol.*, *57*(201), 67–76.
Ritz, C., T. L. Edwards, G. Durand, A. J. Payne, V. Peyaud, and R. C. A. Hindmarsh (2015), Potential sea-level rise from Antarctic ice-sheet instability constrained by observations, *Nature*, *528*, 115–118, doi:10.1038/nature16147.
Robel, A. A., C. Schoof, and E. Tziperman (2016), Persistence and variability of ice-stream grounding lines on retrograde bed slopes, *Cryosphere*, *10*(4), 1883–1896, doi:10.5194/tc-10-1883-2016.
Rosier, S. H. R., G. H. Gudmundsson, and J. A. M. Green (2014), Insights into ice stream dynamics through modelling their response to tidal forcing, *Cryosphere*, *8*(5), 1763–1775, doi:10.5194/tc-8-1763-2014.
Rosier, S. H. R., G. H. Gudmundsson, and J. A. M. Green (2015), Temporal variations in the flow of a large Antarctic ice stream controlled by tidally induced changes in the subglacial water system, *Cryosphere*, *9*(4), 1649–1661, doi:10.5194/tc-9-1649-2015.
Schoof, C. (2005), The effect of cavitation on glacier sliding, *Philos. R. Soc. A*, *461*(2055), 609–627, doi:10.1098/rspa.2004.1350.
Scott, J., H. Gudmundsson, A. Smith, R. Bingham, H. Pritchard, and D. G. Vaughan (2009), Increased rate of acceleration on Pine Island Glacier strongly coupled to changes in gravitational driving stress, *Cryosphere*, *3*, 125–131.
Sergienko, O. V., T. T. Creyts, and R. C. A. Hindmarsh (2014), Similarity of organized patterns in driving and basal stresses of Antarctic and Greenland ice sheets beneath extensive areas of basal sliding, *Geophys. Res. Lett.*, *41*, 3925–3932, doi:10.1002/2014GL059976.

Shapero, D. R., I. R. Joughin, K. Poinar, M. Morlighem, and F. Gillet-Chaulet (2016), Basal resistance for three of the largest greenland outlet glaciers, *J. Geophys. Res. Earth Surf.*, *121*, 168–180, doi:10.1002/2015JF003643.

Smith, A. M., T. A. Jordan, F. Ferraccioli, and R. G. Bingham (2013), Influence of subglacial conditions on ice stream dynamics: Seismic and potential field data from Pine Island Glacier, West Antarctica, *J. Geophys. Res. Solid Earth*, *118*, 1471–1482, doi:10.1029/2012JB009582.

Stokes, C. R., C. D. Clark, O. B. Lian, and S. Tulaczyk (2007), Ice stream sticky spots: A review of their identification and influence beneath contemporary and palaeo-ice streams, *Earth Sci. Rev.*, *81*(3–4), 217–249, doi:10.1016/j.earscirev.2007.01.002.

Tsai, V. C., A. L. Stewart, and A. F. Thompson (2015), Marine ice-sheet profiles and stability under Coulomb basal conditions, *J. Glaciol.*, *61*(226), 205–215, doi:10.3189/2015JoG14J221.

Tulaczyk, S. (2006), Scale independence of till rheology, *J. Glaciol.*, *52*(178), 377–380.

Tulaczyk, S., W. B. Kamb, and H. F. Engelhardt (2000a), Basal mechanics of Ice Stream B, West Antarctica 1. Till mechanics, *J. Geophys. Res.*, *105*(B1), 463–481.

Tulaczyk, S., W. B. Kamb, and H. F. Engelhardt (2000b), Basal mechanics of Ice Stream B, West Antarctica 2. Undrained plastic bed model, *J. Geophys. Res.*, *105*(B1), 483–494.

Van Liefferinge, B., and F. Pattyn (2013), Using ice-flow models to evaluate potential sites of million year-old ice in Antarctica, *Clim. Past*, *9*(5), 2335–2345, doi:10.5194/cp-9-2335-2013.

Vaughan, D. G., and R. Arthern (2007), Why is it hard to predict the future of ice sheets?, *Science*, *315*(5818), 1503–1504, doi:10.1126/science.1141111.

Vieli, A., and A. J. Payne (2003), Application of control methods for modelling the flow of Pine Island Glacier, West Antarctica, *Ann. Glaciol.*, *36*(1), 197–204.

Weertman, J. (1957), On the sliding of glaciers, *J. Glaciol.*, *3*(21), 33–38.

Wilkens, N., J. Behrens, T. Kleiner, D. Rippin, M. Rückamp, and A. Humbert (2015), Thermal structure and basal sliding parametrisation at Pine Island Glacier a 3-D full-Stokes model study, *Cryosphere*, *9*(2), 675–690, doi:10.5194/tc-9-675-2015.

Wingham, D. J., D. W. Wallis, and A. Shepherd (2009), Spatial and temporal evolution of Pine Island Glacier thinning, 1995–2006, *Geophys. Res. Lett.*, *36*, L17501, doi:10.1029/2009GL039126.